DRAFT VERSION NOVEMBER 8, 1999
Preprint typeset using LATEX style emulateapj

RADIO EMISSION FROM 3D RELATIVISTIC HYDRODYNAMIC JETS: OBSERVATIONAL EVIDENCE OF JET STRATIFICATION

MIGUEL-ANGEL ALOY[1], JOSÉ-LUIS GÓMEZ[2], JOSÉ-MARÍA IBÁÑEZ[1], JOSÉ-MARÍA MARTÍ[1] AND EWALD MÜLLER[3]

Draft version November 8, 1999

ABSTRACT

We present the first radio emission simulations from high resolution three dimensional relativistic hydrodynamic jets, which allow for a study of the observational implications of the interaction between the jet and external medium. This interaction gives rise to a stratification of the jet where a fast spine is surrounded by a slow high energy shear layer. The stratification, and in particular the large specific internal energy and slow flow in the shear layer largely determines the emission from the jet. If the magnetic field in the shear layer becomes helical (e.g., resulting from an initial toroidal field and an aligned field component generated by shear) the emission shows a cross section asymmetry, in which either the top or the bottom of the jet dominates the emission. This, as well as limb or spine brightening, is as function of the viewing angle and flow velocity, and the top/bottom jet emission predominance can be reversed if the jet changes direction with respect to the observer, or presents a change in velocity. The asymmetry is more prominent in the polarized flux, because of field cancellation (or amplification) along the line of sight. Recent observations of jet cross section emission asymmetries in the blazar 1055+018 can be explained assuming the existence of a shear layer with a helical magnetic field.

Subject headings: galaxies: jets – hydrodynamics – radiation mechanisms: non-thermal – methods: numerical – relativity

1. INTRODUCTION

The development of high-resolution multidimensional relativistic hydrodynamic codes has provided a tool which allows to simulate the (synchrotron) radio emission from parsec-scale relativistic jets (Gómez et al. 1995, 1997; Komissarov & Falle 1996, 1997; Mioduszewski, Hughes & Duncan 1997), obtaining a better understanding of the physics involved in the jets of active galactic nuclei and their enviroments. It has also been used to successfully explain the structure of particular sources (e.g., 3C 120, Gómez et al. 1998a,b; 3C 454.3, Gómez, Marscher & Alberdi 1999).

In this Letter we study, for the first time, the radio emission properties of three-dimensional relativistic hydrodynamic jet models. In particular, we focus on the observational consequences of the interaction between the relativistic jet and the surrounding medium, which leads to the development of a shear layer. Such shear layers (with distinct kinematical properties and magnetic field configuration) appear naturally in some models of jet formation (Sol, Pelletier, & Asseo 1989) and have been invoked in the past by several authors (Komissarov 1990, Laing 1996, Laing et al. 1999) in order to account for a number of observational characteristics of FRI radio sources. However, the physical nature of the shear layer is still largely unknown. Recently, Swain, Bridle & Baum (1998) have found evidence of shear layers in FRII radio galaxies (3C353), and Attridge, Roberts & Wardle (1999) have inferred a two-component structure in the parsec scale jet of the source 1055+018.

2. JET STRATIFICATION: BEAM AND SHEAR LAYER

To study the emission properties of relativistic jets we have used the high resolution three dimensional relativistic hydrodynamic jet model of Aloy et al. (1999a, hereafter A99). The model is characterized by a beam-to-external proper rest-mass density ratio η = 0.01, a beam Mach number M_b = 6.0, and a beam flow speed $v_b = 0.99c$ (c is the speed of light) corresponding to a beam Lorentz factor of $\Gamma \sim 7$. An ideal gas equation of state with an adiabatic exponent $\gamma = 5/3$ is assumed to describe both the jet matter and the ambient gas. The beam is considered to be in pressure equilibrium with the ambient medium. Non-axisymmetry was triggered by means of a helical velocity perturbation of 1% amplitude and with a period of 3.0 R_b/c (where R_b is the initial beam radius) imposed at the nozzle. We refer the reader to (Aloy et al. 1999b) where a detailed description of the hydrodynamical code can be found.

The jet model is characterized by a two-component structure (Fig. 1) with a fast ($\Gamma \sim 7$) inner jet and a slower ($\Gamma \sim 1.7$) shear layer with high specific internal energy. The shear layer is defined as the region where the beam particle fraction is between 0.2 and 0.95, and is marked in Fig. 1 by white contours. As discussed in A99, the formation of the shear layer is dominated by the numerical viscosity inherent to the hydrodynamic code and not by the turbulent shear. Inspite of this fact, the computed jet models still allow to study the physics of shear layers in relativistic jets and their observational consequences. The width of the shear layer, Δr_l, increases from $\Delta r_l \sim 0.2R_b$ near $z = 0$ to $\Delta r_l \sim 0.65-1.0R_b$ at $z = 68R_b$. This broadening of the shear layer is due to a loss of momentum from the inner jet. As shown in A99, the axial component of the momentum of the beam particles decreases by 30% within the first 60 R_b. This loss of momentum causes a decrease of the Lorentz factor in the inner jet with values $\sim$ 5.8, 5.3, and 4.8 at z = 25, 50, and 68 R_b, respectively.

[1]Departamento de Astronomía y Astrofísica, Universidad de Valencia, 46100 Burjassot (Valencia), Spain. miguel.a.aloy@uv.es; jose.m.ibanez@uv.es; Jose-Maria.Marti@uv.es

[2]Instituto de Astrofísica de Andalucía, CSIC, Apartado 3004, 18080 Granada, Spain. jlgomez@iaa.es

[3]Max-Planck-Institut für Astrophysik, Karl-Schwarzschild-Str. 1, 85748 Garching, Germany. ewald@mpa-garching.mpg.de

3. EMISSION PROPERTIES

The emission properties of large scale jets in AGNs can be studied by computing the radio (synchrotron) emission from relativistic hydrodynamic jet models (see Gómez et al. 1995,1997 and references therein for a complete description of the model). For this, we assume that the particle and energy density of the non-thermal electrons is a constant fraction of the simulated thermal gas. No significant variations from this proportionality are expected to be found within the jet, since the radiative loses and particle accelerations in our model are small. The internal energy among the relativistic non-thermal electrons is distributed following a power law. The magnetic energy is set to be locally proportional and significantly smaller than the particle energy density, hence being dynamically negligible. Different *ad hoc* distributions of the magnetic field in the jet spine and shear layer can therefore be considered. In our model we assume that the magnetic field of the jet consists of two components. A toroidal field present both in the jet spine and the shear layer, and a second component (in equipartition with the toroidal field) aligned in the shear layer and radial in the jet spine. The aligned component in the shear layer could arise from the shear between the jet and the external medium, while the radial field in the jet spine may be due to transverse shocks (i.e., Attridge, Roberts & Wardle 1999). The resulting projected magnetic field is aligned in the shear layer and is perpendicular in the jet spine, as suggested by several observations (Laing 1996; Swain, Bridle & Baum 1998; Attridge, Roberts & Wardle 1999). In order to reproduce the observed relatively low degrees of polarization, an extra randomly oriented magnetic field component (containing 60% of the total magnetic field energy) is assumed both for the shear layer and jet spine.

The Stokes parameters that determine the emission are calculated by integrating the synchrotron transfer equations along columns parallel to the line of sight accounting for the appropriate relativistic effects, such as Doppler boosting and light aberration. Light–travel time delays have been ingnored assuming that the jet is stationary. This is a plausible approximation for the case of the slow evolving large scale jets.

Since only the jet material is expected to radiate, the energy density computed with the hydro code has been weighted with the beam particle fraction. In addition, as we are only interested in studying the emission properties of the stratified jet (beam and shear layer), we can neglect the relatively small contribution to the emission that can arise from the jet cocoon by limiting the calculations to values of the beam particle fraction larger than 0.2. We also ignore the emission from the hot spot, which due to its relatively young evolved state would out shine the rest of the jet, i.e. we have limited the calculations to the inner $68R_b$.

3.1. *Total and polarized emission as a function of the viewing angle*

Because of the highly relativistic speeds in the jet, the emission is mainly determined by the observing viewing angle, θ, through the Doppler factor and light aberration. Figures 2 and 3 show the computed emission from the hydrodynamic model of A99 corresponding to a viewing angle of 50° and 10°, respectively. The emission is computed for an optically thin observing frequency, and spectral index of the electrons of 2.4.

For relatively large viewing angles (Fig. 2) the jet emission is limb brightened. This is in part due to the higher specific internal energy in the shear layer, resulting in a larger synchrotron emission coefficient. On the other hand, the Doppler factor $\delta = \Gamma^{-1}(1-\beta\cos\theta)^{-1}$ (where $\Gamma = 1/\sqrt{(1-\beta^2)}$ and β is the jet flow velocity in units of the speed of light) can either enhance or cancel the limb brightening depending on the value of θ. Because of the jet velocity stratification (see Fig. 1), for relatively large viewing angles the fast jet spine suffers a larger amount of dimming than the shear layer, enhancing the limb brightening. For our jet model, with a mean $\Gamma \sim 7$ in the jet spine, this effect is maximized for $\theta \sim 50°$, for which the shear layer emission is boosted while the jet spine is dimmed (see the panel with the Doppler factor in Fig. 2). Cross section profiles of the jet emission at different viewing angles are plotted in Fig. 4, where the limb brightening effect can be observed more easily. For small viewing angles, as corresponding to Fig. 3, the jet spine emission is boosted, while the shear layer emission appears dimmed. Details of the jet spine can be observed, as for instance two recollimation shocks located at $26R_b$ and $50R_b$. The jet emission then becomes spine brightened, instead of limb brightened, as observed in Figs. 3 and 4.

The same arguments apply to the polarized flux, and we therefore obtain similar limb brightening for large viewing angles, and spine brightening for smaller values. As a result of the helical field in the shear layer, the apparent orientation of the magnetic field at the jet edges is parallel to the jet axis. For the jet spine, the toroidal and radial components of the magnetic field yield a net polarization perpendicular to the jet axis. As shown in Figs. 2 and 4, for relatively large angles the aligned component of the helical magnetic field in the shear layer projects into the jet spine partially canceling its field, yielding a smaller net polarization, thereby stressing the limb brightening. Rails of low polarization can be observed where the apparent magnetic field rotates between being parallel (in the shear layer) to being perpendicular to the jet axis, as observed in 3C 353 (Swain, Bridle & Baum 1998).

Some of the kinematic and physical properties of the jet can be deduced by analyzing the jet/counter jet emission ratio, plotted in Fig. 5 for the jet model of Fig. 2. The jet deceleration is apparent from a progressively decrease in the total flux ratio along the jet axis. The velocity stratification across the jet is also visible as a decrease of the flux ratio close to the jet edges, that is, in the shear layer. This is visible in the inner jet region, while further down the jet, when the jet spine and shear layer velocities are more similar (due to the jet deceleration), the jet/counter jet flux ratio is more uniformly distributed across the jet. The slower velocity in the shear layer and its high emission coefficient result in a smaller integrated flux ratio between the jet and counter jet than for the case of a "naked" high velocity jet spine (see also Komissarov 1990). This is because the shear layer emission is less affected by the viewing angle through the Doppler factor.

3.2. *Jet cross section emission asymmetry*

Because of the helical magnetic field structure in the shear layer, an asymmetry in the emission appears across the jet. This asymmetry is more pronounced in the polarized emission, and is a function of the viewing angle, as shown in Fig. 4. In order to understand this effect we need to study the variation across the jet of the angle between the magnetic field and the line of sight *in the fluid frame*, ϑ. The synchrotron radiation coefficients are a function of the sine of this angle, and asymmetries in the distribution of ϑ will be translated into the emission maps. In order to compute ϑ we need to Lorentz transform the line of sight from the observer's to the fluid's frame (see e.g., Rybicki & Lightman

1979)

$$\sin\theta' = \frac{\sin\theta}{\Gamma(1-\beta\cos\theta)} \quad , \quad \cos\theta' = \frac{\cos\theta-\beta}{(1-\beta\cos\theta)}$$

where θ' is the viewing angle in the fluid frame. Consider a helical magnetic field with a pitch angle ϕ, measured with respect to the jet axis. The angles ϑ^t and ϑ^b (where superscripts t and b refer to the top and bottom of the jet, respectively) add 2ϕ (note that $\vartheta^{t,b}$ is always defined as positive). Therefore, as long as ϕ is different from zero or $\pi/2$, i.e. the field is neither purely aligned nor toroidal, the factor $\sin\vartheta^{t,b}$ in the synchrotron radiation coefficients will introduce an asymmetry in the jet emission. This asymmetry will reach a maximum value for a helical magnetic field with $\phi=\pi/4$, as the one considered here. However, independently of the helix pitch angle, the predominance between $\sin\vartheta^t$ and $\sin\vartheta^b$ will reverse at $\theta'=\pi/2$, which corresponds to a viewing angle in the observer's frame of $\cos\theta_r=\beta$. For a helical field oriented clockwise as seen in the direction of flow motion (i.e., the aligned component of the field is parallel to the jet flow), and for $\theta'<\pi/2$ the bottom of the jet will show larger emission, while for $\theta'>\pi/2$ the top of the jet will be brighter (the opposite is true for a helical field oriented counterclockwise, i.e. $\phi>\pi/2$). The maximum asymmetry will be obtained for $\theta'=\phi$ and $\theta'=\pi-\phi$, and the fastest transition (with changing θ') between top/bottom emission predominance will be obtained for ϕ close to $\pi/2$, i.e. when little aligned field is present.

In the model we are considering, the shear layer has a mean $\Gamma\sim 1.7$, and therefore $\theta_r\sim 36°$. Smaller angles will show bottom jet dominance in emission, while for larger values the top of the jet will appear brighter. This is more clearly visible in Fig. 4. Note also that for the counter jet the helical field rotates opposite to the main jet, and therefore the jet asymmetry emission reverses. This is particularly well observed in the plot of the polarized emission ratio between the jet and counter jet of Fig. 5.

Although the $\sin\vartheta$ factor affects both the total and the polarized emission, the asymmetry is more clearly present in the polarized flux (see Figs. 2, 4 and 5). This is due to: i) The presence of a randomly oriented magnetic field component, which renders the magnetic field distribution more homogeneous in the jet and diminishes the asymmetry. ii) Smaller values of ϑ, independently whether present at the top or the bottom of the jet, always represent a larger variation of the magnetic field orientation along the line of sight. In practice this represents a larger degree of randomness in the magnetic field along the integration columns, decreasing the net polarization.

It is interesting to note that for $\theta\sim\theta_r$, small changes in the jet velocity or the viewing angle will produce a flip in the top/bottom jet emission dominance. For fast jets, θ_r will be accordingly small, and we will be biased towards observing jets with top emission predominance (as long as the helical field rotates clockwise as seen in the direction of flow motion).

An interpretation of the polarization observations of the blazar 1055+018 by Attridge, Roberts & Wardle (1999) can be obtained in terms of the model presented here. For that, we need to assume that 1055+018 is oriented close to θ_r, and contains a shear layer with a helical field. If the helical field is oriented clockwise, the polarized emission observed at the top of the jet in inner regions would require that initially $\theta>\theta_r$, or $\theta'>\pi/2$. To obtain the opposite situation further down the jet, θ' has to become smaller than $\pi/2$, and for that either θ decreases, or θ_r increases, which requires that β decreases. A third less plausible possibility is that the helical field in the shear layer changes orientation, i.e. the pitch angles becomes larger that $\pi/2$. Therefore, we can successfully explain the flip in the top/bottom orientation of the polarization asymmetry in 1055+018 if the jet bends towards the observer, or if it decelerates. Attridge, Roberts & Wardle (1999, and references therein) report the existence of bends in the jet of 1055+018. This supports our hypothesis, but at the location of the flip in the polarization emission asymmetry the jet spine emission decreases abruptly, contrary to what would be expected in the case of a bend towards the observer which should increase the jet spine emission by differential Doppler boosting. Attridge, Roberts & Wardle (1999) obtained significantly larger apparent velocities for components closer to the core suggesting a deceleration along the jet. Therefore, this suggests our hypothesis of jet deceleration as the most plausible for the sudden change in the polarization predominance between the top and bottom of the jet in 1055+018, since a jet deceleration will decrease the Doppler boosting, and hence the jet spine emission as observed. A relatively small aligned field (helical pitch angle close to $\pi/2$) will help to obtain such a fast flip in the polarization asymmetry with a relatively small jet deceleration.

This research was supported by Spain's Dirección General de Enseñanza Superior (DGES) grants PB97-1164 and PB97-1432. MAA expresses his gratitude to the Conselleria d'Educació i Ciència de la Generalitat Valenciana for a research fellowship. We thank A. Alberdi for comments that improved the manuscript.

REFERENCES

Aloy, M. A., Ibáñez, J. M., Martí, J. M., & Müller, E. 1999a, ApJS, 122, 151
Aloy, M. A., Ibáñez, J. M., Martí, J. M., Gómez, J. L., & Müller, E. 1999b, ApJ, 523, L125
Attridge, J. M., Roberts, D. H., & Wardle, J. F. C. 1999, ApJ, 518, L87
Gómez, J. L., Martí, J. M., Marscher, A. P., Ibáñez, J. M., & Marcaide, J. M. 1995, ApJ, 449, L19
Gómez, J. L., Martí, J. M., Marscher, A. P., Ibáñez, J. M., & Alberdi, A. 1997, ApJ, 482, L33
Gómez, J. L., Marscher, A. P., Alberdi, A., Martí, J. M., & Ibáñez, J. M. 1998a, ApJ, 499, 221
Gómez, J. L., Marscher, A. P., Alberdi, A., Martí, J. M., Ibáñez, J. M., & Marchenko, S. G. 1998b, in ASP Conf. 159, BL Lac Phenomenon, ed. L. O. Takalo, & A. Sillanpää (San Francisco: ASP), 435
Gómez, J. L., Marscher, A. P., & Alberdi, A. 1999, ApJ, 522, 74
Komissarov, S. S. 1990. Sov. Astron. Lett. 16(4), 284
Komissarov, S. S., & Falle, S. A. E. G. 1996, in ASP Conf. 100, Energy Transport in Radio Galaxies and Quasars, ed. P. E. Hardee, A. H. Bridle, & J. A. Zensus (San Francisco: ASP), 165
Komissarov, S. S., & Falle, S. A. E. G. 1997, MNRAS, 288, 833
Laing, R. A. 1996, in ASP Conf. 100, Energy Transport in Radio Galaxies and Quasars, ed. P. E. Hardee, A. H. Bridle, & J. A. Zensus (San Francisco: ASP), 241
Laing, R. A., Parma, P., de Ruiter, H. R., & Fanti, R. 1999, MNRAS, 306, 513
Mioduszewski, A. J., Hughes, P. A., & Duncan, G. C. 1997, ApJ, 476, 649
Rybicki, G., Lightman, A. 1979. Radiative Processes in Astrophysics. Wiley, New York, p. 110
Sol, H., Pelletier, G., & Asseo, E. 1989, MNRAS, 237, 411
Swain, M. R., Bridle, A. H., & Baum, S. A. 1998, ApJ, 507, L29

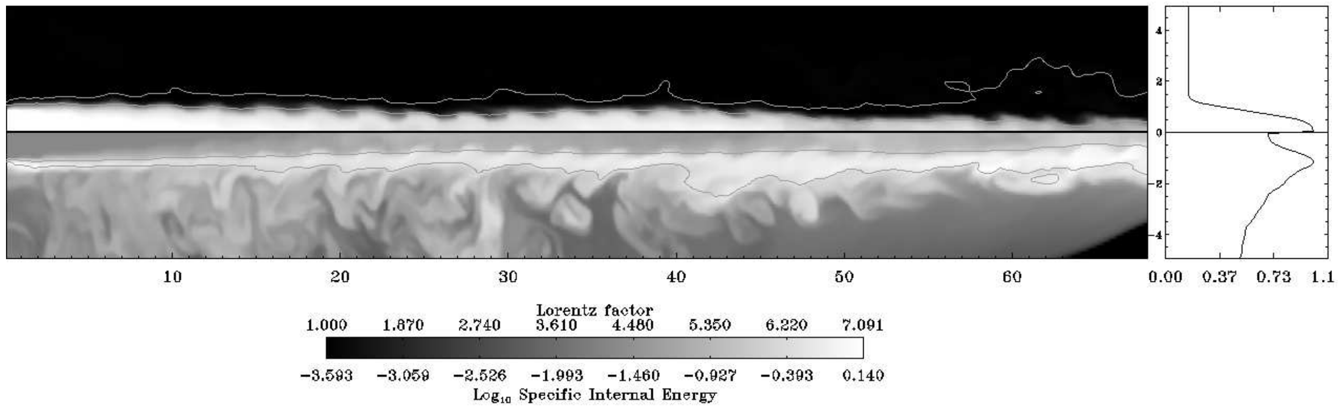

FIG. 1.— Cuts of the Lorentz factor (top half panel) and specific internal energy (bottom half panel) distributions of the hydrodynamic model along the plane $y = 0$. White contours representing constant values of the beam particle fraction (0.95 for the innermost contour, 0.2 for the outermost one) are used to characterize the shear layer. The two panels at the right show the average (along lines x =constant) of the corresponding distributions across the jet.

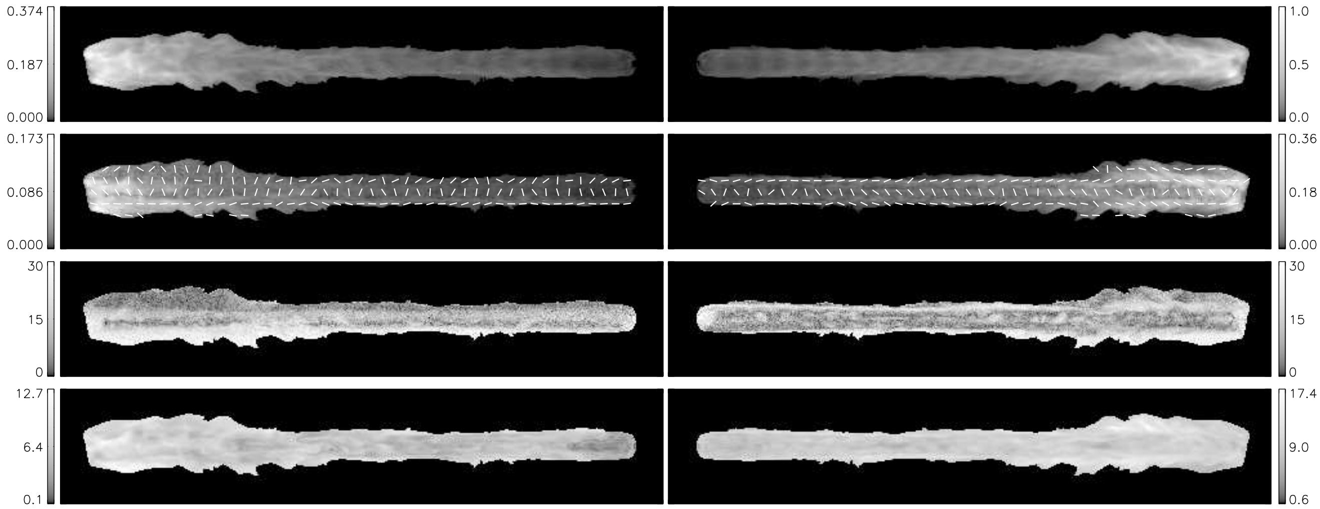

FIG. 2.— From top to bottom the panels show the total intensity, the polarized intensity, the degree of polarization, and mean Doppler factor for a jet viewed at an angle of 50° (right panels) and its counter jet (left panels). Averages along the line of sight for each pixel, using the emission coefficient as a weight, have been used to plot the Doppler factor. The total and polarized intensities (in units normalized to the maximum of the main jet total intensity) are plotted on a square root scale. The bars in the polarized intensity panels show the direction of the magnetic field.

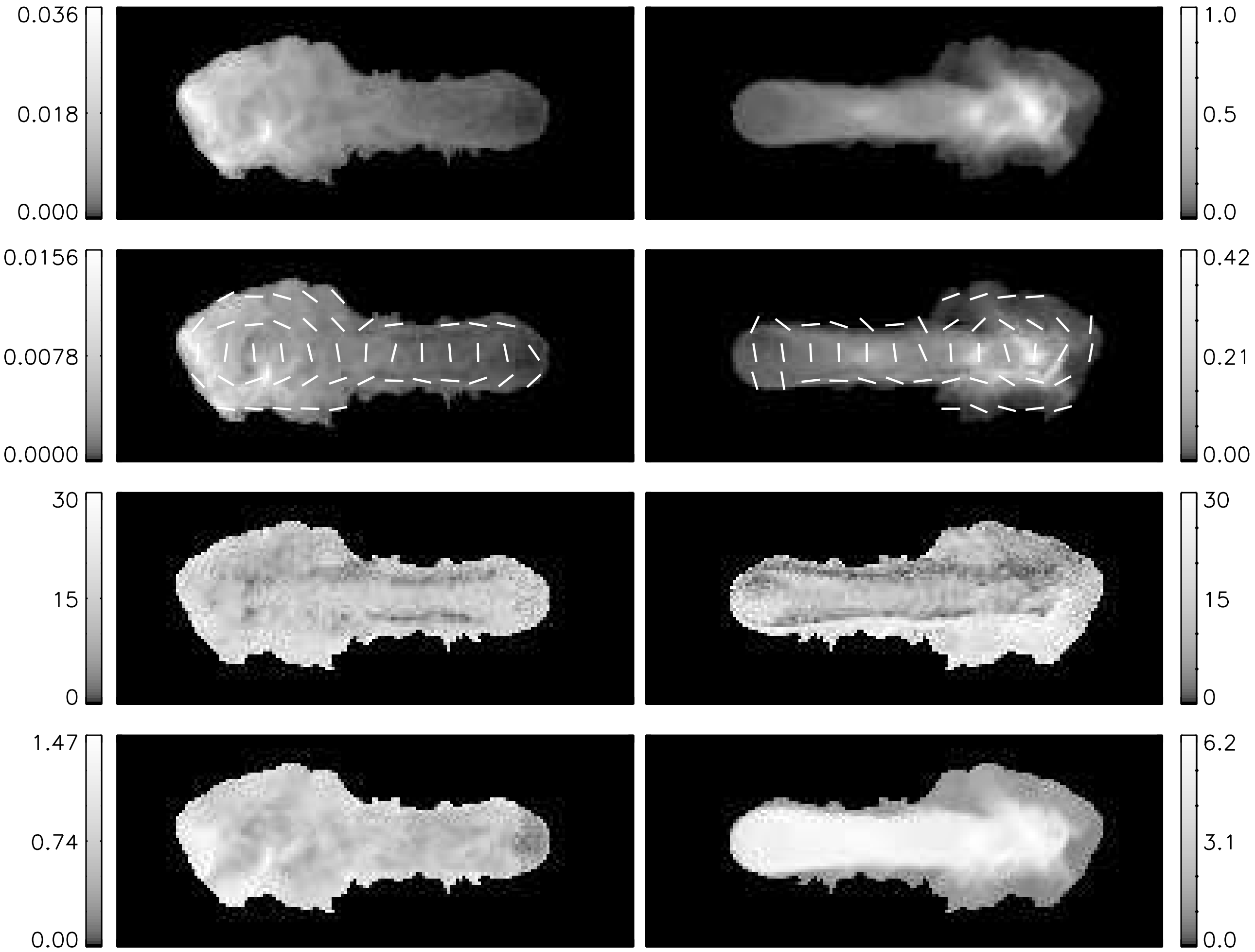

FIG. 3.— Same as Fig. 2, but for a viewing angle of 10°.

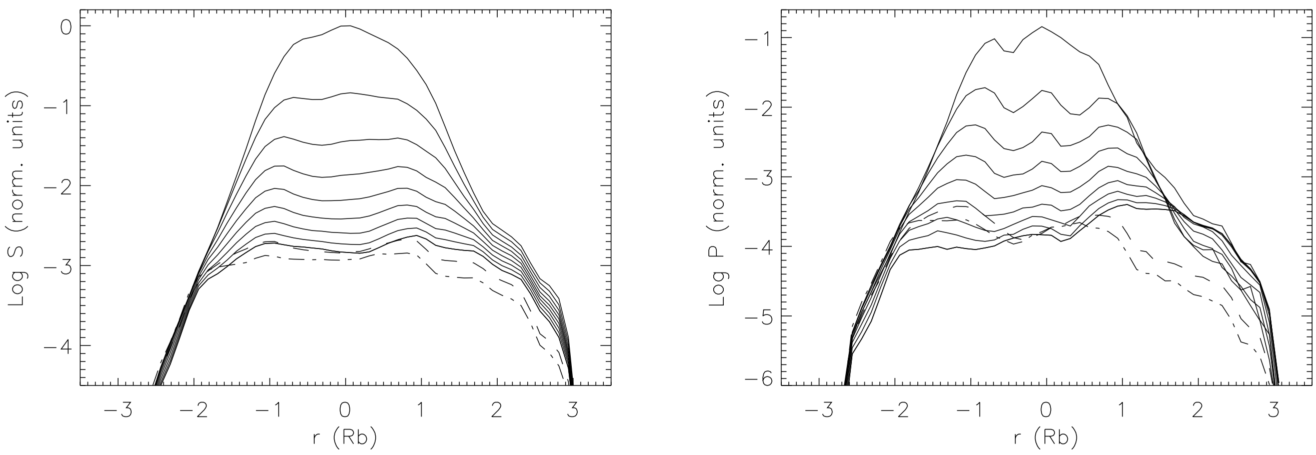

FIG. 4.— Logarithm of the integrated total (*left*) and polarized (*right*) intensity across the jet for different viewing angles. Lines are plotted in intervals of 10° between an angle of 10° (top line in both plots) and 90° (showing a progressive decrease in emission). Dashed (dot dashed) lines correspond to an observing angle of -130° (-170°). Positive beam radii correspond to the top in the images of Figs. 2 and 3. Units are normalized to the maximum total intensity.

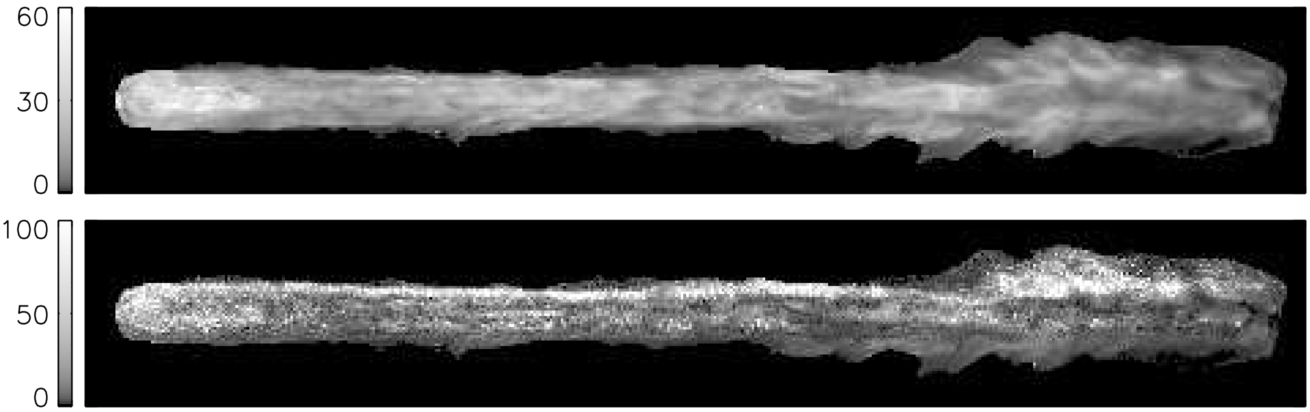

FIG. 5.— Total (*top*) and polarized (*bottom*) intensity jet/counter jet ratios for the jet models of Fig. 2. The polarized ratio is saturated at 100.